Preprints.org

Article

Not peer-reviewed version

Valosin-Containing Protein Contributes to Plexiform Neurofibroma Formation and Represents a Novel Therapeutic Target

Lalitha Gopalan [†], Youjin Na [†], Liang Wu, Ashley Hall, Mi-Ok Kim, Eva Dombi, Sara Szabo, Nancy Ratner, Gang Huang, Jianqiang Wu [*]

Posted Date: 9 March 2026

doi: 10.20944/preprints202603.0600.v1

Keywords: neurofibromin; plexiform neurofibroma; Schwann cell; p97/VCP; CB-5083; PD0325901

Preprints.org is a free multidisciplinary platform providing preprint service that is dedicated to making early versions of research outputs permanently available and citable. Preprints posted at Preprints.org appear in Web of Science, Crossref, Google Scholar, Scilit, Europe PMC.

Copyright: This open access article is published under a Creative Commons CC BY 4.0 license, which permit the free download, distribution, and reuse, provided that the author and preprint are cited in any reuse.

Preprints.org (www.preprints.org) | NOT PEER-REVIEWED | Posted: 9 March 2026 doi:10.20944/preprints202603.0600.v1

Disclaimer/Publisher's Note: The statements, opinions, and data contained in all publications are solely those of the individual author(s) and contributor(s) and not of MDPI and/or the editor(s). MDPI and/or the editor(s) disclaim responsibility for any injury to people or property resulting from any ideas, methods, instructions, or products referred to in the content.

Article

Valosin-Containing Protein Contributes to Plexiform Neurofibroma Formation and Represents a Novel Therapeutic Target

Lalitha Gopalan [1,†], Youjin Na [1,†], Liang Wu [1], Ashley Hall [1], Mi-Ok Kim [2], Eva Dombi [3], Sara Szabo [4], Nancy Ratner [1,5], Gang Huang [6] and Jianqiang Wu [1,5,*]

[1] Division of Experimental Hematology and Cancer Biology, Cancer & Blood Diseases Institute Cincinnati Children's Hospital Medical Center, 3333 Burnet Ave., Cincinnati, OH 45229, USA
[2] Department of Epidemiology and Biostatistics, UCSF, 1450 3rd Street, San Francisco, CA 94143, USA
[3] Pediatric Oncology Branch, National Cancer Institute, Bethesda, MD 20892, USA
[4] Department of Pediatrics and Department of Pediatric Pathology, Cincinnati Children's Hospital Medical Center, University of Cincinnati, Cincinnati, Ohio
[5] Department of Pediatrics, University of Cincinnati College of Medicine, Cincinnati, OH, 45267 USA
[6] Department of Cell Systems and Anatomy, UT Health San Antonio, Joe R. and Teresa Lozano Long School of Medicine, San Antonio, Texas, USA
* Correspondence: jianqiang.wu@cchmc.org; Tel.: 1-513-636-0955
† These authors contributed equally to this work.

Highlights

- VCP interacts with neurofibromin in Schwann cells
- VCP expression is increased in both mouse and human plexiform neurofibroma (PNF)
- VCP contributes to neurofibroma initiation and maintenance
- Targeting inhibition of VCP reduced mouse plexiform neurofibroma growth, suggesting a potential novel therapy for patients with PNFs

Abstract

Neurofibromatosis type 1 (NF1) patients are predisposed to develop plexiform neurofibromas (PNFs). By cross comparison of RNA sequencing and RUNX1-CHIP sequencing data on mouse PNF, we found that transcript encoding the NF1 interacting p97/valosin-containing protein (VCP) gene is overexpressed in PNF. Co-immunoprecipitation confirmed that VCP bounded to neurofibromin. Western blot and immunostaining confirmed VCP protein overexpression in both mouse and human PNFs. Treatment of primary mouse PNF Schwann cells with CB-5083, a p97/VCP inhibitor, led to accumulation of poly-ubiquitinated proteins and generation of irresolvable proteotoxic stress. Pharmacological or genetic inhibition of VCP reduced mouse PNF cell derived sphere number, and genetic inhibition of *Vcp* in Schwann cell precursors decreased tumor-like lesion numbers in a cell transplantation model. In vivo treatment with CB-5083 on the *Nf1*$^{fl/fl}$;*DhhCre* PNF mouse significantly inhibited cell proliferation, increased cell apoptosis and reduced PNF volume. The combination with a MEK inhibitor did not increase efficacy compared to the single agent, supporting the hypothesis that VCP functions in parallel to, and may be modulated by, RAS–MAPK signaling under stress or oncogenic conditions. The significant effects of VCP inhibition in this pre-clinical study suggest a potential novel therapy for patients with PNFs.

Keywords: neurofibromin; plexiform neurofibroma; Schwann cell; p97/VCP; CB-5083; PD0325901

1. Introduction

© 2026 by the author(s). Distributed under a Creative Commons CC BY license.

Preprints.org (www.preprints.org) | NOT PEER-REVIEWED | Posted: 9 March 2026 doi:10.20944/preprints202603.0600.v1

Neurofibromatosis type 1 (NF1) is classified as rare, but of the rare diseases is relatively common, affecting 1 in 2500 people worldwide [1–3]. One of the hallmarks is that about 30-50% of NF1 patients develop plexiform neurofibromas (PNFs), a benign Schwann cell (SC) tumor. PNFs can transform into malignant peripheral nerve sheath tumors, a lethal sarcoma [4–6]. PNFs can be large and locally invasive, and can cause substantial morbidity—including pain, neurologic deficit, motor dysfunction, disfiguration, and even death. The mainstay of PNF therapy, surgery, is sometimes impossible due to tumor integration into nerves in critical anatomic sites. There are two FDA-approved MEK inhibitors (MEKi), selumetinib and mirdametinib, for the treatment of PNFs. These two inhibitors shrink PNFs in 40-70% of NF1 patients, but tumor shrinkage is modest in most tumors, and some tumors regrow when drug is withdrawn [7–9]. In addition, patients receiving MEKi treatment often experience side effects—including elevated creatine phosphokinase, acneiform rash, and paronychia [7,8]. Finally, given that PNF onset is during early childhood [10], taking selumetinib or mirdametinib for life can be problematic due to adherence and side effects issues. Therefore, new effective and durable therapeutic strategies are urgently needed.

Valosin-containing protein (VCP, also called p97) is a homohexamer consisting of an N-terminal domain, two ATPase (D1 and D2) domains, a flexible linker region, and a C-terminal domain. VCP is an AAA+ ATPase that, by interaction with a wide variety of partners and cofactors, regulates proteostasis and multiple other cellular processes (e.g., lysosomal dynamic stability) [11–13]. VCP, usually through its ATPase activity, regulates ubiquitination [13,14]. VCP also regulates autophagy [15,16]. In neurons, VCP interacts directly with neurofibromin, the NF1 gene encoding protein [17], and heterozygous *Nf1* (*Nf1*$^{+/-}$) neurons regulate protein synthesis in endoplasmic reticulum (ER) via VCP [15]. In addition to regulating proteostasis, VCP also suppresses apoptosis by unfold protein response in normal and tumor cells [18–22]. Importantly, in many human tumors, VCP mRNA and protein are elevated, and multiple in vivo studies strongly suggest that VCP promotes tumor growth [13,23,24].

To develop effective and durable therapies for PNF, it is critical to understand the signaling pathways controlling PNF formation and growth — particularly the MEK-independent or MEK synergistic pathways. In this study, we showed that VCP interacts with neurofibromin in SCs and its protein was overexpressed in both mouse and human PNFs. Treatment of primary mouse PNF SCs with CB-5083, a p97/VCP ATPase inhibitor (VCPi), led to accumulation of poly-ubiquitinated proteins and generation of irresolvable proteotoxic stress. Pharmacological or genetic inhibition of VCP reduced mouse neurofibroma-sphere number, and genetic inhibition of *Vcp* in Schwann cell precursors (SCPs) decreased tumor-like lesion numbers in a cell transplantation model. In vivo treatment with CB-5083 on the *Nf1*$^{fl/fl}$;*DhhCre* mouse of PNF significantly inhibited cell proliferation, increased cell apoptosis and reduced neurofibroma volume, suggesting targeting VCP might be an alternative therapeutic strategy for patients with PNFs.

2. Materials and Methods

2.1. Animals

The animal care and use committees of Cincinnati Children's Hospital Medical Center approved all animal procedures. Institutional Animal Care and Use Committee (IACUC) guidelines were followed with animal subjects. Mice were housed in temperature- and humidity- controlled facilities on 12-hour dark-light cycles with free access to food and water. The floxed -*Nf1* mouse (*Nf1*$^{fl/fl}$) has been described previously [25] and was on a mixed 129/BL/6 background. The *DhhCre* transgenic mouse harbors a nuclear-localized *Cre* recombinase gene under control of the mouse desert hedgehog (*Dhh*) promoter/regulatory regions and was maintained on C57/BL/6 background [26]. We bred *DhhCre* mice onto *Nf1*$^{fl/fl}$ mice to obtain the F1 generation (*Nf1*$^{fl/+}$;*DhhCre*$^{+}$); we bred male F1 mice with female *Nf1*$^{fl/fl}$ mice to obtain *Nf1*$^{fl/fl}$;*DhhCre* mice. Genotyping was performed as described previously [27].

© 2026 by the author(s). Distributed under a Creative Commons CC BY license.

Preprints.org (www.preprints.org) | NOT PEER-REVIEWED | Posted: 9 March 2026 doi:10.20944/preprints202603.0600.v1

2.2. Mouse MRI and Volumetric Measurements

Mouse MRI and volumetric measurements were performed as described [14]. Specifically, *Nf1*$^{fl/fl}$;*DhhCre* PNF-bearing mice were scanned by MRI at 5, 7 and 9 months of age to monitor PNFs using 7T Bruker Biospec system equipped with 400 G/cm gradients in the Imaging Resource Center at Cincinnati Children's Hospital. MRI volumetric measurements were used to determine the tumor volume change as described previously [28]. All volumes were reported as combined tumor volume in an individual mouse. Mouse treatment groups were blind to the person who performed the volumetric measurements.

2.3. Reagents

CB-5083 (ChemGood, Henrico, VA, USA) and PD0325901 (mirdametinib, Selleck Chemicals, Houston, TX, USA) were dissolved in 0.5% [w/v] methylcellulose (Neta Scientific, Hainesport, NJ, USA; #SIAL-M0262) solution with 0.2% [v/v] polysorbate 80 [Tween 80] (Fisher Scientific, Waltham, MA, USA; # BP338-500) for mouse dosing. CB-5083 was sonicated at medium level energy for 2 minutes on ice before use.

2.4. Immunoprecipitation Assay

Passage two embryonic day 12.5 WT mouse SCs ($1x10^8$) were lysed in Np-40 buffer as described [29], and 750 μg of the total protein lysate was used for immunoprecipitation with a neurofibromin antibody (Santa Cruz Biotechnology, Dallas, TX, USA; # sc-398267, 1:200) or normal mouse IgG control Ab (Santa Cruz Biotechnology; #sc-2025, 1:200). The immunoprecipitated complexes were separated by SDS-PAGE and transferred to PVDF membranes for immunoblotting with detection anti-NF1 (Cell Signaling Technology, Danvers, MA, USA; #14623, 1:1000) and VCP (Proteintech, Rosemont, IL, USA; # 10736-1-AP, 1:2000) antibodies.

2.5. Western Blots

Mouse spheres, PNFs or WT mouse dorsal root ganglia (DRG)/nerve lysates were used for western blots as described [30]. For immunoblotting, we used the following antibodies: VCP (Proteintech; # 10736-1-AP, 1:2000); pERK (Cell Signaling Technology; #4370, 1:2000), ERK (Cell Signaling Technology; #4695, 1:2000),Ubiquitin (Cell Signaling Technology; #58395, 1:1000), CHOP (Cell Signaling Technology; #5554, 1:1000), GAPDH (Cell Signaling Technology; #3683, 1:3000), or β-actin (Cell Signaling Technology; #5125, 1:5000). Antibody binding to the membrane was visualized using a chemiluminescent detection system (EMD Millipore, Burlington, MA, USA; #WBKLS0500).

2.6. Generation of shRNAs and Lentiviral Transduction

We purchased two VCP specific shRNA-expressing lentiviral plasmids (TRCN0000008410 [#10] and TRCN0000008413[#11]) from Sigma-Aldrich (St. Louis, MO, USA) and produced lentivirus particles by transient co-transfection of 293T cells as described [31]. After concentration of the lentiviral particles using a commercial Lenti-X concentrator (Takara Bio Inc, Shiga, Japan; # 631231), we determined the titer of the concentrated lentivirus.

2.7. Mouse PNF Cell-Derived Sphere Culture and Treatment

Mouse PNF cell-derived sphere culture was performed as described [30,32]. Briefly, we cut PNFs into around 1 mm^3 piece and dissociated them in 20 ml L-15 (Mediatech, Herndon, VA, USA; #10-045-CV) containing 0.5 mg/ml collagenase type 1 (Worthington Biochemical, Lakewood, NJ, USA; #LS004196) and 2.5 mg/ml Dispase protease type II (Roche, Indianapolis, IN,USA; #C756V28) at 37 °C for 3 hours with 200rpm shaking. We plated trypan blue negative single cells at 4 x 10^4 cells per well in 24-well low-binding plates (Fisher Scientific, # Corning 3473) with 1mL medium containing DMEM:F-12 (3:1) containing 20 ng/ml rhEGF (R&D Systems, Minneapolis, MN,USA; # 236-EG-200),

© 2026 by the author(s). Distributed under a Creative Commons CC BY license.

Preprints.org (www.preprints.org) | NOT PEER-REVIEWED | Posted: 9 March 2026 doi:10.20944/preprints202603.0600.v1

20 ng/ml rh bFGF (PeproTech, Cranbury, NJ; #450-33-50µg), 1% B-27 supplement (Life Technologies, Carlsbad, CA, USA; #17504-044), and 2 mg/ml heparin (Sigma-Aldrich; #H3149-10KU). Spheres were cultured at 37 °C at 5% CO_2. We used secondary spheres for each experiment.

For treatment, we seeded dissociated live cells from primary spheres into 24-well ultra-low attachment plates at a density of 4×10^4 cells/well for 48-72 hours and then treated them with vehicle, CB-5083, sh*Vcp* or sh*NT* lentivirus. For drug treatment, CB-5083 at 0nM, 1nM, 10nM, 100nM, 1,000nM, and 10,000nM were used. After 4 days, the sphere numbers were counted using a phase-contrast microscopy (Olympus CKX41, Tokyo, Japan). For lentivirus treatment, we transduced secondary PNF cell- derived spheres with purified sh*Vcp* or sh*NT* (Sigma-Aldrich) at the multiplicity of infection of 1:10 for 3 days and collect sphere for western blot, and at 4 days for sphere number counting.

2.8. Tumorigenesis Assay in NSG Mice

We treated *Nf1*$^{fl/fl}$*;DhhCre* mouse PNF- derived secondary spheres with sh*NT* or *shVcp (#11)* lentivirus at multiplicity of infection of 1:10 for 3 days and dissociated them into single cells. We subcutaneously injected 5×10^5 dissociated sphere cells/injection within 33% Matrigel (Fisher Scientific; #CB-40234) into right flanks of NSG mice (males and females, Harlan, Indianapolis, IN) as described [30]. After 3 months, we dissected lesions under a dissection microscope to confirm visible tumors and counted tumor number.

2.9. Quantitative Real-Time PCR (qRT-PCR)

Total RNA was isolated from mouse tissues using the Qiagen RNeasy Kit (Hilden, Germany). The cDNA was synthesized using the High-Capacity cDNA Reverse Transcription Kit (Thermo Scientific, Waltham, MA, USA; #4368814). QRT-PCR was performed using SYBR Green (Applied Biosystems, Foster City, CA, USA; #4368708). The ΔΔCt method was used for calculation. Data represented three independent experiments with triplicate in each sample. The following mouse primers were used: *Svip:* forward: 5′-GCTTCCAGACTTAGTGCCTTTA-3′, reverse; 5′-CGTCCTACGGACATGTAACTT-3′. Tublin: forward: 5′-CATTCAGGGCTCCATCAAAT-3′, reverse :5′-GCCCTACAACTCCATCCTCA-3′

2.10. Immunohistochemistry and Immunofluorescence

Paraformaldehyde -fixed, paraffin-embedded tissue blocks were sectioned at 10 µm. Tissue sections were de-paraffinized in xylene, rehydrated in serial concentrations of ethanol, and then boiled in citrate buffer (pH 6.0) for antigen retrieval. Tissues were permeabilized with 0.2% triton-X100/PBS (TBST) for 30 minutes and washed with PBS three times. After blocking with 10% normal goat serum (Jackson ImmunoResearch, West Grove, PA, USA; #005-000-121) in TBST, the sections were incubated with primary antibodies: Ki67 (Cell Signaling Technology, # 12202S, 1:200), VCP (Proteintech, # 10736-1-AP, 1:200), and SVIP (Abcam, Cambridge, MA, USA; #ab122590, 1:250) overnight at 4 °C and then treated with biotinylated or Fluorescence dye-conjugated secondary antibodies for 1 hr. The biotinylated antibody was detected with horseradish peroxidase-conjugated streptavidin (Elite ABC, Vector Laboratories, Burlingame, CA, USA; #PK-6100) and cell nuclei were stained with hematoxylin. Fluorescently labeled sections were stained with 0.1 µg/ml DAPI (Fisher Scientific; #62248) for nuclei counting and then mounted in Fluoromount G slide mounting medium (Electron Microscopy Sciences, Hatfield, PA, USA; 17984-25). Images were captured on a Nikon C2 Confocal microscope.

2.11. TUNEL Assay

TUNEL assay was performed according to Roche In situ cell death detection kit instruction (TMR red, Roche Diagnostics Gmbh, Mannheim, Germany; Ref# 12156792910), on deparaffinized

© 2026 by the author(s). Distributed under a Creative Commons CC BY license.

Preprints.org (www.preprints.org) | NOT PEER-REVIEWED | Posted: 9 March 2026 doi:10.20944/preprints202603.0600.v1

sections. We stained nuclei with DAPI. We counted TUNEL⁺ cells and DAPI nuclei in at least three cross sections per sample. Data were presented as an average percentage of TUNEL⁺ cells per sample.

2.12. Statistical Analysis

We used unpaired 2-tailed Student's *t*-tests to analyze the significance of cell population percentages or relative mRNA expression when two samples were compared. We used one-way ANOVA to analyze the significance of cell proliferation, apoptosis and sphere numbers per well. Data was reported as the mean ± SD in at least three independent experiments or samples. $P<0.05$ was considered significant. We used a mixed-effects model to analyze PNF growth. P values were generated with a random-effects model analysis on log-transformed tumor volume data using the SAS mixed procedure [33]. For the in vivo cell transplantation experiment, we used Fisher's exact test for p-value.

3. Results

3.1. VCP Interacts with Neurofibromin in SCs and Is Overexpressed in Mouse and Human PNFs

We previously showed that ER stress protein homoeostasis is unbalanced in PNF SC/SCPs [29]. Given the increased protein synthesis and activation of ER stress pathways observed in PNF cells, we decided to examine upstream components of the ER proteostasis machinery. By comparing PNF RNA sequencing and PNF SC RUNX1-CHIP sequencing data on mouse PNF, we found that transcript encoding the NF1 interacting p97/VCP gene was overexpressed in PNF. To determine if VCP interacts with neurofibromin in SCs, we performed immunoprecipitation on mouse WT SCs. Western blot confirmed that anti-NF1 immunoprecipates contained VCP while was not present in IgG control (**Figure 1A**), indicating VCP specifically interacts with neurofibromin in SCs. To check if VCP expression is altered upon loss of *Nf1*, we performed western blots on PNFs from 7-month-old *Nf1*$^{fl/fl}$*;DhhCre* mice and age matched WT DRG. We detected increased expression of VCP in PNFs compared to WT mouse DRG (**Figure 1B**). Immunofluorescence staining on human PNF showed that there was significantly increased VCP expression cells compared to normal human nerve controls (**Figure 1C, 1D**). These data suggests that VCP is present in SCs.

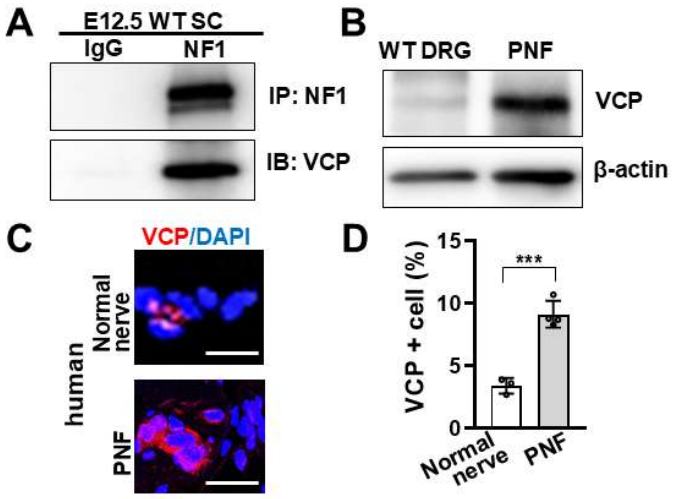

Figure 1. VCP interacts with neurofibromin in Schwann cells and is overexpressed in mouse and human PNFs. **A**. Interaction between neurofibromin and VCP in wild type (WT) mouse Schwann cells showing VCP interacts

© 2026 by the author(s). Distributed under a Creative Commons CC BY license.

Preprints.org (www.preprints.org) | NOT PEER-REVIEWED | Posted: 9 March 2026 doi:10.20944/preprints202603.0600.v1

with neurofibromin. IP: neurofbromin, immunoblot: VCP. Control: IgG. **B**. Western blot on 7 months old *Nf1$^{fl/fl}$;DhhCre* mouse PNF and age matched WT mouse DRG showing VCP expression is increased in PNF. Loading control: β-actin. **C.** Representative image of immunofluorescence staining of VCP (red) on normal human nerve (top) and human PNF (bottom). DAPI staining nuclei. Bar: 20μM. **D.** Quantification of VCP^{+} percentage cells in normal human nerve (left, white bar, n=3) and human PNFs (right, gray bar, n=4) showing significant increase in PNF compared to normal human nerve. ***p<0.0001.

3.2. RUNX1 Binding to SVIP Indirectly Regulates VCP Expression

We decided to determine how VCP expression is increased in PNFs.

We previously showed that RUNX1 contributes to PNF formation [34]. Western blot of VCP on *Nf1$^{fl/fl}$;DhhCre* and *Runx1$^{fl/fl}$;Runx3$^{fl/fl}$;Nf1$^{fl/fl}$;DhhCre (Runx1/3-cKO; Nf1$^{fl/fl}$;DhhCre)* mouse PNFs showed decreased VCP protein expression in *Runx1/3-cKO; Nf1$^{fl/fl}$;DhhCre* (**Figure 2A**). Because RUNX1 has not been noted to interact with VCP, we explored potential downstream targets of RUNX1 that might interact with VCP, by integrating 3 published data sets: *Runx1/3-cKO; Nf1$^{fl/fl}$;DhhCre* RNAseq differential gene expression [34], Runx1 CHIP-seq peaks [34]. and known VCP-interacting proteins [12]. The small VCP interacting protein (*Svip*) was the only gene common to all 3 data sets (**Figure 2B**). This suggests that loss of NF1 increases RUNX1 expression, which in turn promotes RUNX1 binding to SVIP, thereby indirectly regulating VCP expression. In fact, *Svip* mRNA expression was significantly increased in *Runx1/3-cKO; Nf1$^{fl/fl}$;DhhCre* PNFs (vs *Nf1$^{fl/fl}$;DhhCre*) (**Figure 2C**), and increased relative mRNA expression data was validated by qRT-PCR (**Figure 2D**). We were unbale to identify an anti-SVIP antibody for immunofluorescence staining in mouse PNF. Therefore, we checked SVIP expression levels in human PNFs. Consistent with the anti-correlated expression of SVIP and VCP [11], immunofluorescence staining on human PNFs showed decreased SVIP protein expression compared with normal human nerve controls (**Figure 2E**).

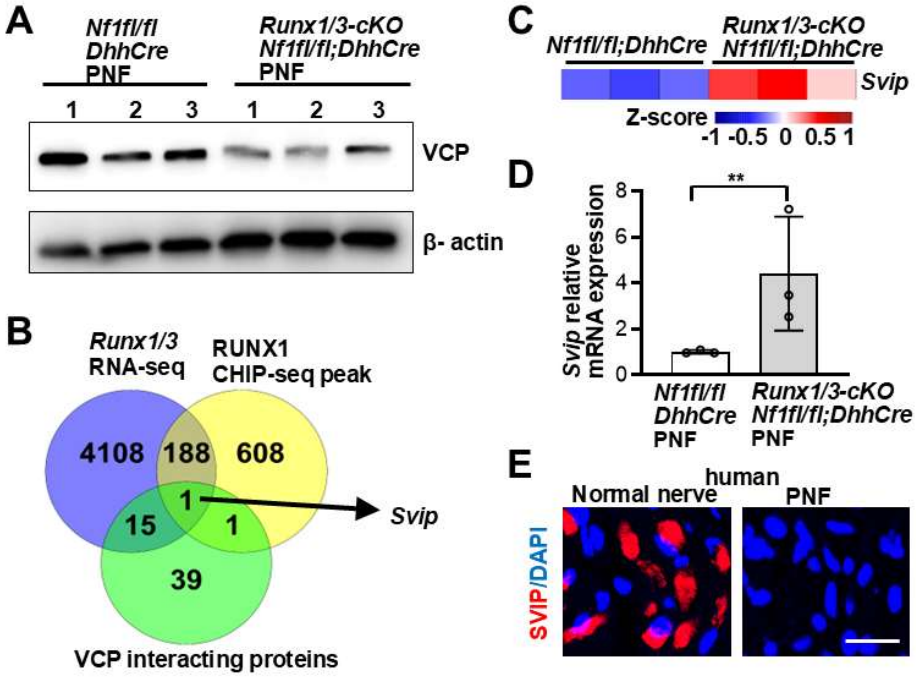

Figure 2. RUNX1 binding to SVIP indirectly regulates VCP expression. A. Western blot of VCP in *Nf1$^{fl/fl}$;DhhCre* (n=3) and *Runx1$^{fl/fl}$;Runx3$^{fl/fl}$;Nf1$^{fl/fl}$;DhhCre* (*Rnux1/3-cKO;Nf1$^{fl/fl}$;DhhCre)* (n=3) mouse PNFs. Loading control, β-actin. **B.** Venn diagram of shared gene expression of 3 data sets (*Runx1/3* RNA-seq, RUNX1 CHIP-seq peak, and VCP interaction proteins). **C,D.** Heatmap (**C**) and qRT-PCR (**D**) of *Svip* expression in PNFs from *Nf1$^{fl/fl}$;DhhCre*

© 2026 by the author(s). Distributed under a Creative Commons CC BY license.

Preprints.org (www.preprints.org) | NOT PEER-REVIEWED | Posted: 9 March 2026 doi:10.20944/preprints202603.0600.v1

and *Runx1/3-cKO;Nf1-cKO* mice. n=3 mice/group. *, $p<0.05$. **E.** Representative image of SVIP immunofluorescence (Red) in human PNF (right) vs normal nerve (left). DAPI stains nuclei. Bar: 20μM.

3.3. Overwhelming Proteotoxic Stress by Targeting VCP Inhibits Cell Growth and Induces Protein Ubiquitination in PNF SCs

Since the anti-tumor activity of MEK inhibitors (PD0325901 or selumetinib) is not cytotoxic and is not durable post-treatment [7,8,35,36], we tested whether targeting VCP is cytotoxic for NF1 PNF cells. The D2 domain of VCP is the primary driver of ATPase activity and conformational changes, and CB-5083 is a selective VCP D2 domain inhibitor [37]. CB-5083 treatment led to a dramatic dose-dependent growth inhibition in PNF-derived SCs compared to WT SCs; importantly, the cytotoxic effect on WT SCs was relatively modest (**Figure 3A**). Similarly, protein ubiquitination increased in CB-5083-treated PNF derived SCs 6 hours after treatment and was also dose dependent (**Figure 3B)**; at 500 nM the difference in protein ubiquitination between WT and PNF cells was most dramatic, suggesting a potential therapeutic dose window. Interestingly, CB-5083 did not change p-ERK expression (an MAPK inhibition readout) even at 700nM, suggesting that VCP might be MEK/ERK pathway independent or regulated by MEK/ERK pathway. To verify that CB-5083 selectively affects the VCP ATPase activity in this setting, we performed ATPase quantification assays on CB-5083 treated mouse WT and PNF SCs. ATPase activity inhibition was similar in both 0.5μm and 1μM CB-5083 treated WT SCs. On the contrary, ATPase activity was significantly reduced in 1μM CB-5083 treated PNF SCs compared to vehicle control (**Figure 3C**).

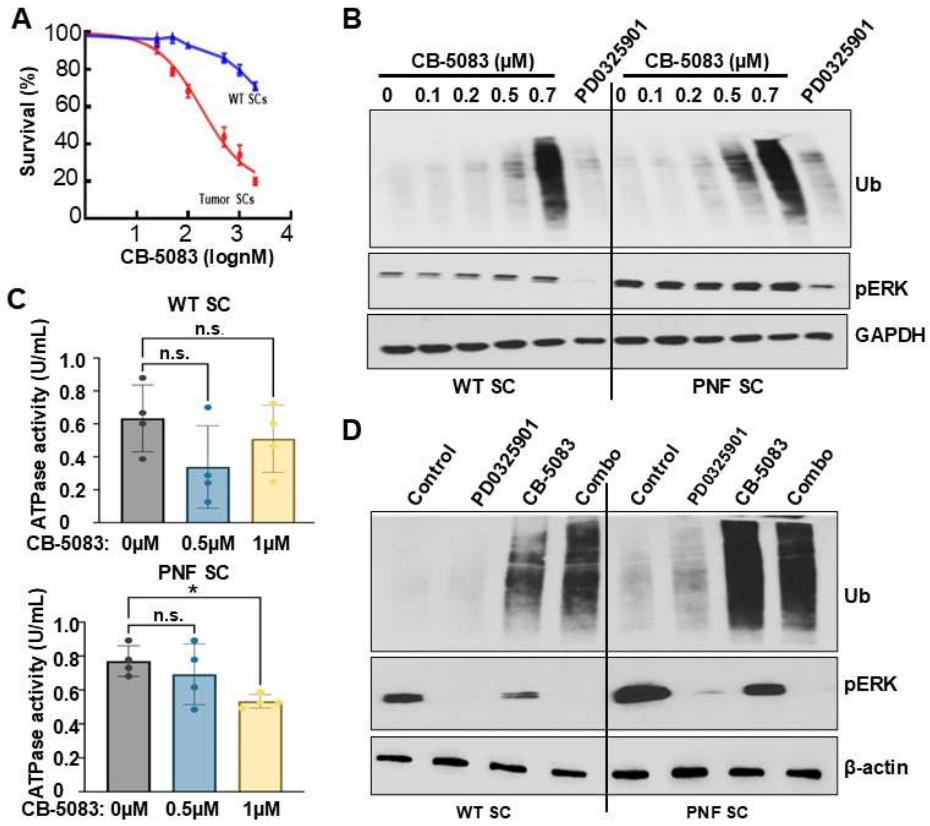

Figure 3. Overwhelming proteotoxic stress by targeting VCP inhibits cell growth and inducing ubiquitination in PNF SCs. A. MTS assay showing Inhibition of VCP differentially inhibits WT (blue) and PNF (red) Schwann cells growth. **B**. Western blots showing dose response and differentially ubiquitination effects following 6-hour treatment with CB-5083 on mouse Schwann cells derived from WT DRG or PNF. PD0325901 was used for comparison. Loading controls, GAPDH. **C**. Quantification of ATPase activity in CB-5083–treated

© 2026 by the author(s). Distributed under a Creative Commons CC BY license.

Preprints.org (www.preprints.org) | NOT PEER-REVIEWED | Posted: 9 March 2026 doi:10.20944/preprints202603.0600.v1

WT or PNF Schwann cells for 6 hours showing 1μM CB-5083 treatment significantly reduces PNF Schwann cell ATPase activity (n=4/group). * p<0.05, n.s.; no significant difference. **D**. Western blots showing protein ubiquitination effects or p-ERK activity change following 6-hour treatment with CB-5083 (0.5 μM), PD0325901 (1μM) alone, or in combo on mouse Schwann cells derived from WT DRG or PNF. Combo= 0.5 μM CB-5083 + PD0325901 1μM. Loading controls, β-actin. .

We next tested if VCPi + MEKi combination treatment leads to additive effects. We treated WT and PNF SCs with control, PD0325901 (1μM), CB-5083 (0.5μM), or the combination for 6 hours. Western blot showed that the combination treatment inhibited p-ERK expression and induced ubiquitination simultaneously; MEKi reduced p-ERK expression while CB-5083 induced protein ubiquitination. Consistently, CB-5083 +/- PD0325901 showed stronger effects on protein ubiquitination in PNF SCs vs WT SCs (**Figure 3D).**

3.4. Pharmacological and Genetic Inhibition of VCP Decreases Mouse PNF Cell-Derived Sphere Number In Vitro

Schwann cell precursors (SCPs) are the cell of origin for PNF. To test if inhibition of VCP affects SCP growth and/or tumorigenesis, we used a neurofibroma sphere culture system, in which SCPs grow as self-renewing spheres that can be passaged in vitro for 2-3 passages [38]. CB-5083 inhibited sphere formation (numbers) in a dose-dependent manner (**Figure 4A**). Eexposure (4 days) to CB-5083 at 100nM led accumulation of protein ubiquitination (**Figure 4B**), which was not observed after short term (6 hours) treatment at this dose (**Figure 3B**). To verify that this inhibitory effect was specifically caused by VCP, we treated *Nf1*$^{fl/fl}$*;DhhCre* mouse PNF SC-derived secondary spheres with two different *Vcp* sh-RNAs (sh*Vcp#10* and sh*Vcp#11*) for 4 days. Each sh*Vcp* significantly decreased sphere numbers compared to sh*NT* control (**Figure 4C**). VCP knockdown was confirmed by western blot (**Figure 4D**). These results indicates that VCP is important for SCP growth.

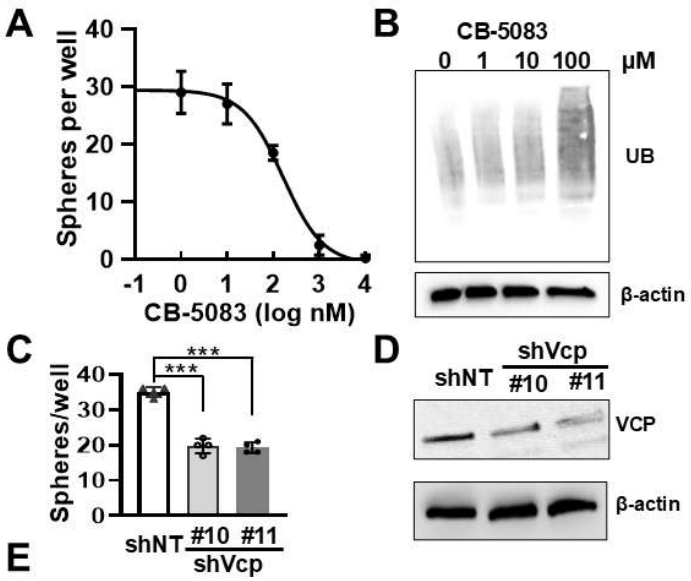

virus	Tumors/injections	P value (Fisher's exact test)
shNT	10/10	0.033
shVcp	5/10	

© 2026 by the author(s). Distributed under a Creative Commons CC BY license.

Preprints.org (www.preprints.org) | NOT PEER-REVIEWED | Posted: 9 March 2026 doi:10.20944/preprints202603.0600.v1

Figure 4. Pharmacological and genetic inhibition of VCP decreases mouse Schwann cell precursor growth in vitro and tumorigenesis in vivo. A. Dose response curve showing decreased numbers of mouse neurofibroma-derived spheres by CB-5083 treatment for 4 days. Three independent experiments were performed. **B.** Western blot showing protein ubiquitination on spheres from A. Loading control: β-actin. **C.** Quantification showing mouse neurofibroma-derived sphere numbers significantly reduced in two sh*Vcp*-expressing lentivirus treated spheres for 4 days. Three independent PNFs were used. Each experiment was performed in triplicates. ***, $p<0.001$. **D.** Western blot showing efficiently inhibited VCP protein expression by sh*Vcp* in mouse PNF cell-derived spheres. **E.** Decreased tumor-like lesion formation rate by transplantation of sh*Vcp*-lentivirus treated sphere compared to that of sh*NT* control-treated sphere. A Fisher Exact test was performed.

3.5. VCP Contributes to Neurofibroma Initiation

To test whether VCP reduction in neurofibroma sphere numbers decreases tumorigenic potential in vivo, we dissociated 3-day sh*Vcp#11* or sh*NT* lentivirus-treated *Nf1*$^{fl/fl}$*;DhhCre* mouse PNF-derived secondary tumor sphere cells into single cell and injected them subcutaneously into NSG mice. Three months after transplantation, all mice (10 of 10) grafted with sh*NT*-treated spheres showed neurofibroma-like micro-lesions, while only 5 of 10 NSG mice showed detectable lesions in mice transplanted with sh*Vcp*-treated sphere cells ($p< 0.05$) (**Figure 4F**). Thus, VCP loss compromised neurofibroma initiation in this assay. Global *Vcp* knockout mice die during embryonic development [39]. We tried to delete VCP in SCc and SCPs using conditional *VCP*$^{fl/fl}$ mice [40] to determine the role of *Vcp* in PNF initiation and/or maintenance, unfortunately the *VCP*$^{fl/fl}$*;Nf1*$^{fl/fl}$*;DhhCre* mice died before post-natal day 2 (not shown). Therefore, genetic deletion of *Vcp* in SCs and SCPs in PNF-bearing mice is not feasible for evaluating its role in PNF development.

3.6. Short- Term CB-5083 + PD0325901 Treatment Significantly Inhibites Cell Proliferation and Induces Cell Death

Treatment of MEK inhibitors, mirdametinib (PD0325901) and selumetinib, delays PNF growth, but the effects are modest on most of the PNFs and some PNFs re-grow after stopping treatment [7,8,35,36]. Based on our in vitro combination results (**Figure3D**), we tested if VCPi might provide additional benefit in vivo. We first determined the maximum tolerated dose for CB-5083. Prior reports showed that CB-5083 at 100 mg/kg daily treatment for one week induces protein ubiquitination and cell apoptosis and reduced tumor growth in vivo [41,42]. This dose (in single or combination treatment) was toxic to *Nf1*$^{fl/fl}$*;DhhCre* mouse after daily treatment for 2 months. After dose de-escalation, we confirmed that the maximum tolerated dose for CB-5083 was 80mg/kg in this model. All mice survived with less than 20% weight loss in either single reagent or combination treatment (not shown). To evaluate in vivo efficacy, we treated *Nf1*$^{fl/fl}$*;DhhCre* mouse with vehicle control, CB-5083 (80 mg/kg), PD0325901 (1.5 mg/kg), or combination [CB-5083 (80mg/kg) + PD0325901 (1.5mg/kg)] for 5 days by oral gavage, the PNFs were removed 2 hours after last dose for analysis. Ki67 immunolabeling revealed decreased cell proliferation following either PD0325901 or combination treatment, but not in VCB-5083 only treatment group (**Figure 5A**, **5B**). There was no significant difference in cell death between control and PD0325901 alone; in fact, we have never observed increased cell death following PD0325901 treatment either in vivo or in vitro [35,36]. Importantly, the combination treatment showed significantly more TUNEL$^+$ cells than either CB-5083 or PD0325901 alone (**Figure 5C, 5D**).

© 2026 by the author(s). Distributed under a Creative Commons CC BY license.

Preprints.org (www.preprints.org) | NOT PEER-REVIEWED | Posted: 9 March 2026 doi:10.20944/preprints202603.0600.v1

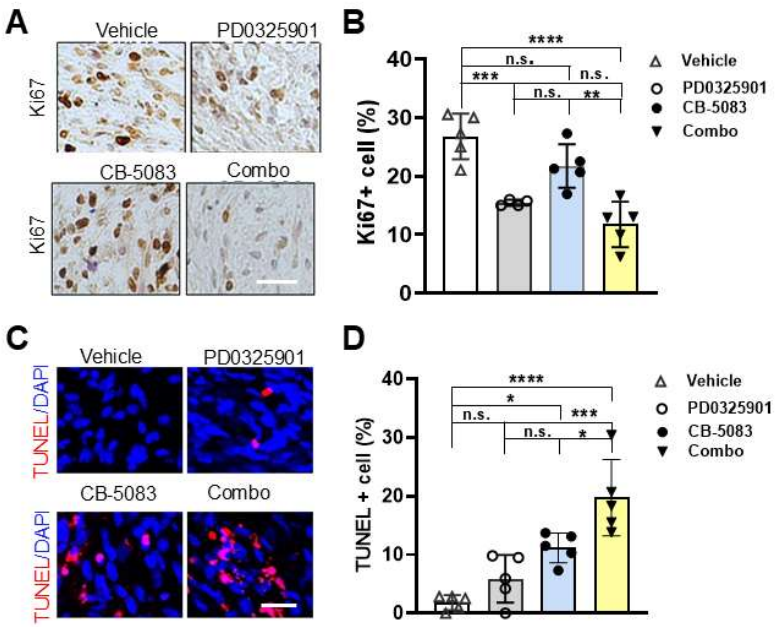

Figure 5. Short-term CB-5083 + PD0325901 treatment significantly inhibits cell proliferation and induces cell death. A. Representative images of Ki67 on PNFs removed from *Nf1*$^{fl/fl}$*;DhhCre* mice received CB-5083 (80 mg/kg), PD0325901 (1.5 mg/kg), combo, or vehicle control by oral gavage once a day for 5 days (n=5/group). **B.** Quantification of Ki67+ percentage showing differential inhibitory effect on cells. **C**. Representative images of TUNNEL on PNFs removed from *Nf1*$^{fl/fl}$*;DhhCre* mice received CB-5083 (80 mg/kg), PD0325901 (1.5 mg/kg), CB-5083 (80 mg/kg) + PD0325901 (1.5 mg/kg) combination, or vehicle control by oral gavage once a day for 5 days. **D**. Quantification of TUNEL+ percentage showing differential effect on inducing cell death. n=4-5 mice/group. Combo= CB-5083 (80 mg/kg) + PD0325901 (1.5 mg/kg). *, p<0 .05; **, $p < 0.01$; ***, $p < 0.0001$, ***p < 0.00001. Bar: 20μM.

3.7. Long-Term CB-5083 or CB-5083 + PD0325901 Treatment Reduces Tumor Volume, and Inhibits Cell Proliferation, and Induces Cell Death/Protein Ubiquitination

Finally, we assessed the long-term in vivo effects of inhibiting VCP activity with CB-5083 on PNF growth. We treated the *Nf1*$^{fl/fl}$*;DhhCre* mice with CB-5083 (80mg/kg), PD0325901 (1.5mg/kg), combination, or vehicle control using a 5 on, 2 off regimen for 8 weeks. A few mice lost <10% weight during the first two weeks but all regained weight thereafter (data not shown). All mice survived and there were no obvious side morbidities. AS predicted, PD0325901 treatment significantly reduced tumor volume (p<0.0001). Volumetric measurement also showed that the percent tumor volume changes also significantly decreased in CB-5083 or combination treated mice compared to vehicle controls (p=0.037, p<0.0001 respectively) (**Figure 6A).** However, no difference was observed in the CB-5083 + PD0325901 treated group when compared with CB-5083 (p=0.492) or PD0325901 (p=0.435) monotherapy. CB-5083, PD0325901, or combination treatment all significantly reduced the number of Ki67+ proliferating cells compared to vehicle, with the CB-5083 + PD0325901 combination showing the greatest effect. (**Figure 6B, 6C**). TUNEL staining showed CB-5083 or CB-5083 + PD0325901 treatment significantly increased cell death while no difference was detected in PD0325901 treatment group compared to vehicle (**Figure 6D, 6E**). Western blot revealed unfold protein response and ER stress response as evidenced by increased CHOP and protein ubiquitination signal following treatment with VCPi alone, or in combination with MEKi. Importantly, the western blot data also showed that p-ERK was strongly inhibited by the combination treatment (**Figure 6F**).

© 2026 by the author(s). Distributed under a Creative Commons CC BY license.

Preprints.org (www.preprints.org) | NOT PEER-REVIEWED | Posted: 9 March 2026 doi:10.20944/preprints202603.0600.v1

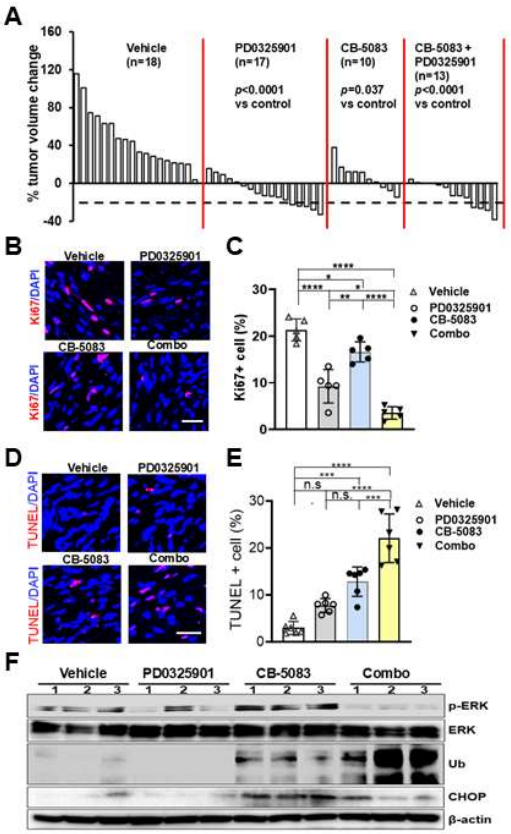

Figure 6. Long-term CB-5083 or CB-5083 + PD0325901 treatment significantly reduced tumor volume by inhibiting cell proliferation and inducing cell death and ubiquitination. A. Waterfall plot showing mouse tumor volume change. Data from each mouse were shown as a single bar. Change in tumor volume was quantified between 7 and 9 months for each individual mouse treated with vehicle (control) (n = 18), PD0325901 (n = 17), CB-5083 (n=10), or CB-5083+ PD0325901 (n=13) for 8 weeks. **B.** Representative images of Ki67 on PNFs removed from *Nf1*$^{fl/fl}$*;DhhCre* mice received CB-5083 (80 mg/kg), PD0325901 (1.5 mg/kg), CB-5083 (80 mg/kg) + PD0325901 (1.5 mg/kg) combination, or vehicle control by oral gavage once a day for 60 days. **C.** Quantification of Ki67+ percentage showing differential inhibitory effect on cells (n=5 mice/group). **D**. Representative images of TUNNEL on PNFs removed from *Nf1*$^{fl/fl}$*;DhhCre* mice received CB-5083 (80 mg/kg), PD0325901 (1.5 mg/kg), CB-5083 (80 mg/kg) + PD0325901 (1.5 mg/kg) combination, or vehicle control by oral gavage once a day for 5 days. **E** Quantification of UNEL+ percentage showing differential effect on inducing cell death. n=6 mice/group. *, p<0 .05; **, p < 0.01; ***, p <0.0001, ***p <0.00001. **F.** Western blot of PNF lysates from 4 different treatments; 3 mice/group. Loading control, β-actin. In B-E, combo= CB-5083 (80 mg/kg) + PD0325901 (1.5 mg/kg). Bar: 20μM.

4. Discussion

VCP is a highly conserved AAA+ ATPase. It has many functions including protein quality control, ER associated degradation and the ubiquitin–proteasome system maintenance. VCP plays a key role in protein homeostasis and cell survival in normal cells. It is believed that cancer cells can hijack this function to survive cell stress. Thus, VCP is increasingly recognized as a pro-tumorigenic factor and biomarker in many cancers, including non-small cell lung cancer, pancreatic cancer, colorectal cancer, bladder cancer, multiple myeloma, melanoma, breast cancer, hepatocellular carcinoma, and ovarian cancer [43,44]. In this study, we showed that VCP interacts with neurofibromin, the NF1 gene encoding protein, in SCs and that its expression is increased in both mouse and human PNFs. The data are consistent with the idea that RAS–MAPK activation in *Nf1*$^{-/-}$

© 2026 by the author(s). Distributed under a Creative Commons CC BY license.

Preprints.org (www.preprints.org) | NOT PEER-REVIEWED | Posted: 9 March 2026 doi:10.20944/preprints202603.0600.v1

cells induce proteostatic stress that increases reliance on VCP to maintain protein homeostasis and cell survival, and thereby supporting PNF growth.

VCP interacts with a wide variety of cofactors to regulate proteostasis. More than 40 proteins that bind to VCP's domains have been identified. These proteins regulate VCP ATPase activity and/or direct VCP to specific location to carry out functions such as DNA repair, membrane trafficking, or cell cycle control [12]. SVIP, a small regulatory protein, localizes on the ER membrane and acts as a key regulator of VCP-mediated processes, including unfold protein response and ER associated degradation. lt has been described as having a tumor suppressor role in glioblastoma [45]. We showed that SVIP expression is reduced in human PNF (**Figure 2E**) and might act as a negative regulator of VCP to contribute to PNF growth, consistent with a tumor suppressor role. Our results suggest that VCP might be either directly regulated by neurofibromin, or that loss of *Nf1* increases *Runx1* expression, which in turn represses *Svip* expression, leading to activation of *Vcp.* It will be important to define which pathway affects VCP expression in PNF in the future.

In PNFs, SCPs contribute to tumor formation. We showed that pharmacological and genetic inhibition of VCP decreases mouse neurofibroma sphere number in vitro. Genetic knock-down *Vcp* significantly reduced tumor like lesion formation in NSG mice (**Figure 4E**), suggesting VCP itself or in coordination with RAS-MAPK signaling contributes to PNF initiation.

VCP contributes to tumor growth suggested that targeting VCP might be a good therapeutic approach. VCP uses energy from ATP hydrolysis to unfold and segregate ubiquitinated protein substrates for degradation. When VCP's ATPase activity is inhibited, ubiquitinated proteins accumulate, leading to cell stress and often initiating programmed cell death (apoptosis). CB-5083, a potent with moderate oral bioavailability VCPi, was identified in 2015. CB-5083 bound to the D2 domain of VCP to inhibit VCP ATPase activity and led to retention of ER associated degradation and generation of irresolvable proteotoxic stress, therefore induced apoptosis. It inhibited tumor growth in hematological xenograft models [41,46]. CB-5083 suppressed osteosarcoma growth and stem cell properties by altering protein homeostasis [47]. Zhang et al. show that pharmacological inhibition of VCP by CB-5083 partially abolished the oncogenic effects of TMEM63A on triple-negative breast cancer progression both in vitro and in vivo [48]. Single-agent CB-5083 inhibited xenografted bladder cancer growth and CB-5083 effectively kills tumor cells and acted as a radio sensitizing agent both in vitro and in vivo [49] and multiple myeloma [50]. Targeting VCP enhanced colorectal cancer therapy through STING stabilization [51]. The differential inhibitory effects between WT SCs and PNF SCs on cell growth (**Figure 3A**) and protein ubiquitination (**Figure 3B**) indicated a potential therapeutic efficacy for PNFs by targeting VCP. We showed that inhibition of VCP significantly reduced PNF growth compared to control (**Figure 6A**), suggesting that VCP might be an alternative therapeutic target.

In vitro CB-5083 + PD0325901 combination treatment resulted in protein ubiquitination and p-ERK inhibition, while single reagent only led to protein ubiquitination (CB-5083) or p-ERK inhibition (PD0325901) (**Figure 3D**), suggesting co-targeting VCP and MEK might provide synthetic lethality. Importantly, we detected increased cell death in either at 5-day or 60-day combination treatment group. Although combination showed a trend of better efficacy, we did not detect significant difference in reducing PNF volume percentage change compared to single reagent PD0325901 or CB-5083 (**Figure6A**). It is possible that: 1) PD0325901 or CB-5083 each has very strong effects on reducing tumor volume, so we did not have enough power (i.e., mouse number) to reach statistical difference. 2) VCP functions in parallel to, or is modulated by, RAS–MAPK signaling under stress or oncogenic condition. 3) Elevated VCP expression is a secondary adaptive response to RAS-MAPK driven stress rather than a direct signaling target. 4) Other unidentified pathway(s) might be involved or compensated in PNF initiation/maintenance upon inhibition of VCP and MEK. 5) The combination did not kill SCPs, the PNF-initiating cells. Future work should focus on identifying the specific cell populations that die in response to CB-5083 or combination treatment.

The first generation VCPi (CB-5083) tested here showed some off-target effect: two phase I clinical trials (NCT02243917 and NCT02223598) were terminated due to adverse effects on vision

© 2026 by the author(s). Distributed under a Creative Commons CC BY license.

Preprints.org (www.preprints.org) | NOT PEER-REVIEWED | Posted: 9 March 2026 doi:10.20944/preprints202603.0600.v1

resulting from inhibition of phosphodiesterase-6 [52]. In 2021, a second-generation VCPi, CB-5339, was developed and it showed efficacy in several multiple AML models [53]. This compound has progressed through early clinical evaluation with the successful completion of a Phase I study in acute myeloid leukemia or myelodysplastic syndrome (NCT04402541), providing important data on safety, tolerability, and pharmacokinetics. A second phase I study on testing the safety of CB-5339 in patients with solid tumors that have spread to other places in the body (advanced) or lymphomas (NCT04372641) was withdrawn for unreported reasons. Overall, these early clinical experiences have informed dose selection and study design, supporting the continued advancement of this inhibitor. It will be interesting to test CB-5339 in our PNF mouse model and compare its effect on PNF growth with that of CB-5083 in the future.

5. Conclusions

It is well established that loss of *Nf1* increases RAS activity, thereby activating the MEK/ERK signaling pathway and contributes to PNF formation. We demonstrate that VCP interacts with neurofibromin. Furthermore, loss of *Nf1* upregulates *Runx1* expression, which binds to SVIP to enhance VCP expression, thereby further contributing to PNF pathogenesis. (Figure 7). VCP expression is increased in both mouse and human PNFs. It might be regulated by and functionally coupled to RAS–MAPK driven SC states. The significant effects of VCP inhibition in this pre-clinical study suggest a potential novel therapy for patients with PNFs.

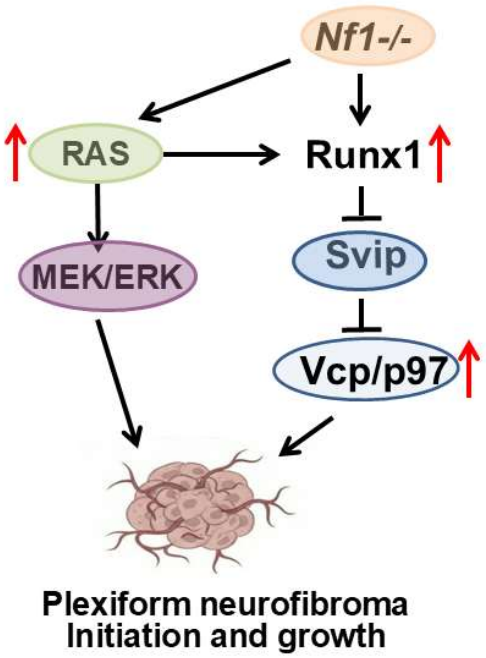

Figure 7. A schematic model of plexiform neurofibroma initiation and growth. Loss of *Nf1* increases RAS activity, thereby activating the MEK/ERK signaling pathway and contributes to PNF formation. In the meantime, loss of *Nf1* upregulates *Runx1* expression, which binds to SVIP to enhance VCP expression, thereby further contributing to PNF pathogenesis.

Author Contributions: Conceptualization: G.H. and J.W. Methodology: L.G., Y. N., L.H., A.H., and S.S. Validation: L.G., Y. N., L.H., and S.S. Formal Analysis: L.G., Y. N., L.H., A.H., and S.S; Investigation: L.G., Y. N., L.H., A.H., and S.S. Resources: N.R and J.W. Data Curation: L.G and Y.N. Writing – Original Draft Preparation: J.W. Writing – Review & Editing: G.H., N.R. and J.W. Visualization: L.G. Supervision: N.R. and J.W. Project Administration: J.W. Funding Acquisition: N.R. and J.W.

© 2026 by the author(s). Distributed under a Creative Commons CC BY license.

Preprints.org (www.preprints.org) | NOT PEER-REVIEWED | Posted: 9 March 2026 doi:10.20944/preprints202603.0600.v1

Funding: This work was supported by NIH R01 NS097233 and University of Cincinnati/Cincinnati Children's Hospital Center for Clinical & Translational Science &Training (CCTST) just in time grant to JW and NS28840 to NR.

Institutional Review Board Statement: The animal care and use committees of Cincinnati Children's Hospital Medical Center approved all animal procedures. Institutional Animal Care and Use Committee (IACUC) guidelines were followed with animal subjects. IACUC #: 2021-0035.

Data Availability Statement: All materials described in the manuscript, including all relevant raw data, will be freely available to any researcher wishing to use them for non-commercial purposes, without breaching participant confidentiality.

Acknowledgments: We thank Ms. Sydney Szuch for performing genotyping on some mice. We thank Dr. Conrad Weihl from the Washington University for providing the *Vcp*$^{fl/fl}$ mice for our experiments.

Conflicts of Interest: For Dr. Dombi: this research was supported in part by the Intramural Research Program of the National Institutes of Health (NIH). The contributions of the NIH authors were made as part of their official duties as NIH federal employees, are in compliance with agency policy requirements, and are considered Works of the United States Government. However, the findings and conclusions presented in this paper are those of the authors and do not necessarily reflect the views of the NIH or the U.S. Department of Health and Human Services. The other authors declare no conflict of interests in relation to the work described.

References

1. Blatt J, Jaffe R, Deutsch M, Adkins J. Neurofibromatosis and childhood tumors. Cancer. 1986;57(6):1225-9.
2. Boyd KP, Korf BR, Theos A. Neurofibromatosis type 1. J Am Acad Dermatol. 2009;61(1):1-14; quiz 5-6.
3. Kallionpää, R.A.; Uusitalo, E.; Leppävirta, J.; Pöyhönen, M.; Peltonen, S.; Peltonen, J. Prevalence of neurofibromatosis type 1 in the Finnish population. *Anesthesia Analg.* **2018**, *20*, 1082–1086, https://doi.org/10.1038/gim.2017.215.
4. Evans, D.G.R.; O'HAra, C.; Wilding, A.; Ingham, S.L.; Howard, E.; Dawson, J.; Moran, A.; Scott-Kitching, V.; Holt, F.; Huson, S.M. Erratum: Mortality in neurofibromatosis 1: in North West England: an assessment of actuarial survival in a region of the UK since 1989. *Eur. J. Hum. Genet.* **2013**, *21*, 1031–1031, https://doi.org/10.1038/ejhg.2013.121.
5. Ratner, N.; Miller, S.J. A RASopathy gene commonly mutated in cancer: the neurofibromatosis type 1 tumour suppressor. *Nat. Rev. Cancer* **2015**, *15*, 290–301, https://doi.org/10.1038/nrc3911.
6. Varan, A.; Şen, H.; Aydın, B.; Yalçın, B.; Kutluk, T.; Akyüz, C. Neurofibromatosis type 1 and malignancy in childhood. *Clin. Genet.* **2015**, *89*, 341–345, https://doi.org/10.1111/cge.12625.
7. Dombi, E.; Baldwin, A.; Marcus, L.J.; Fisher, M.J.; Weiss, B.; Kim, A.; Whitcomb, P.; Martin, S.; Aschbacher-Smith, L.E.; Rizvi, T.A.; et al. Activity of Selumetinib in Neurofibromatosis Type 1–Related Plexiform Neurofibromas. *New Engl. J. Med.* **2016**, *375*, 2550–2560, https://doi.org/10.1056/nejmoa1605943.
8. Gross, A.M.; Wolters, P.L.; Dombi, E.; Baldwin, A.; Whitcomb, P.; Fisher, M.J.; Weiss, B.; Kim, A.; Bornhorst, M.; Shah, A.C.; et al. Selumetinib in Children with Inoperable Plexiform Neurofibromas. *N. Engl. J. Med.* **2020**, *382*, 1430–1442, doi:10.1056/nejmoa1912735.
9. Gross, A.M.; Dombi, E.; Wolters, P.L.; Baldwin, A.; Dufek, A.; Herrera, K.; Martin, S.; Derdak, J.; Heisey, K.S.; Whitcomb, P.M.; et al. Long-term safety and efficacy of selumetinib in children with neurofibromatosis type 1 on a phase 1/2 trial for inoperable plexiform neurofibromas. *Neuro-Oncology* **2023**, *25*, 1883–1894, https://doi.org/10.1093/neuonc/noad086.
10. Nguyen, R.; Kluwe, L.; Fuensterer, C.; Kentsch, M.; Friedrich, R.E.; Mautner, V.-F. Plexiform Neurofibromas in Children with Neurofibromatosis Type 1: Frequency and Associated Clinical Deficits. *J. Pediatr.* **2011**, *159*, 652–655.e2, https://doi.org/10.1016/j.jpeds.2011.04.008.
11. Johnson, A.E.; Orr, B.O.; Fetter, R.D.; Moughamian, A.J.; Primeaux, L.A.; Geier, E.G.; Yokoyama, J.S.; Miller, B.L.; Davis, G.W. SVIP is a molecular determinant of lysosomal dynamic stability, neurodegeneration and lifespan. *Nat. Commun.* **2021**, *12*, 1–17, https://doi.org/10.1038/s41467-020-20796-8.

© 2026 by the author(s). Distributed under a Creative Commons CC BY license.

Preprints.org (www.preprints.org) | NOT PEER-REVIEWED | Posted: 9 March 2026 doi:10.20944/preprints202603.0600.v1

12. Hänzelmann, P.; Schindelin, H. The Interplay of Cofactor Interactions and Post-translational Modifications in the Regulation of the AAA+ ATPase p97. *Front. Mol. Biosci.* **2017**, *4*, 21, https://doi.org/10.3389/fmolb.2017.00021.
13. van den Boom, J.; Meyer, H. VCP/p97-Mediated Unfolding as a Principle in Protein Homeostasis and Signaling. *Mol. Cell* **2018**, *69*, 182–194, doi:10.1016/j.molcel.2017.10.028.
14. Meyer, H.; Bug, M.; Bremer, S. Emerging functions of the VCP/p97 AAA-ATPase in the ubiquitin system. *Nat. Cell Biol.* **2012**, *14*, 117–123, https://doi.org/10.1038/ncb2407.
15. Shih, Y.-T.; Huang, T.-N.; Hu, H.-T.; Yen, T.-L.; Hsueh, Y.-P. Vcp Overexpression and Leucine Supplementation Increase Protein Synthesis and Improve Fear Memory and Social Interaction of Nf1 Mutant Mice. *Cell Rep.* **2020**, *31*, 107835, https://doi.org/10.1016/j.celrep.2020.107835.
16. Bhardwaj, M.; Leli, N.M.; Koumenis, C.; Amaravadi, R.K. Regulation of autophagy by canonical and non-canonical ER stress responses. *Semin. Cancer Biol.* **2019**, *66*, 116–128, https://doi.org/10.1016/j.semcancer.2019.11.007.
17. Wang, H.-F.; Shih, Y.-T.; Chen, C.-Y.; Chao, H.-W.; Lee, M.-J.; Hsueh, Y.-P. Valosin-containing protein and neurofibromin interact to regulate dendritic spine density. *J. Clin. Investig.* **2011**, *121*, 4820–4837, https://doi.org/10.1172/jci45677.
18. Nishimura, N.; Radwan, M.O.; Amano, M.; Endo, S.; Fujii, E.; Hayashi, H.; Ueno, S.; Ueno, N.; Tatetsu, H.; Hata, H.; et al. Novel p97/VCP inhibitor induces endoplasmic reticulum stress and apoptosis in both bortezomib-sensitive and -resistant multiple myeloma cells. *Cancer Sci.* **2019**, *110*, 3275–3287, https://doi.org/10.1111/cas.14154.
19. Braun, R.J.; Zischka, H. Mechanisms of Cdc48/VCP-mediated cell death — from yeast apoptosis to human disease. *Biochim. et Biophys. Acta (BBA) - Mol. Cell Res.* **2008**, *1783*, 1418–1435, https://doi.org/10.1016/j.bbamcr.2008.01.015.
20. Desdicioglu, R.; Sahin, C.; Yavuz, F.; Cayli, S. Disruption of p97/VCP induces autophagosome accumulation, cell cycle arrest and apoptosis in human choriocarcinoma cells. *Mol. Biol. Rep.* **2021**, *48*, 2163–2171, https://doi.org/10.1007/s11033-021-06225-z.
21. Yeo, B.K.; Hong, C.J.; Chung, K.M.; Woo, H.; Kim, K.; Jung, S.; Kim, E.-K.; Yu, S.-W. Valosin-containing protein is a key mediator between autophagic cell death and apoptosis in adult hippocampal neural stem cells following insulin withdrawal. *Mol. Brain* **2016**, *9*, 1–14, https://doi.org/10.1186/s13041-016-0212-8.
22. Zhang, H.; Li, K.; Lin, Y.; Xing, F.; Xiao, X.; Cai, J.; Zhu, W.; Liang, J.; Tan, Y.; Fu, L.; et al. Targeting VCP enhances anticancer activity of oncolytic virus M1 in hepatocellular carcinoma. *Sci. Transl. Med.* **2017**, *9*, https://doi.org/10.1126/scitranslmed.aam7996.
23. Parzych, K.; Saavedra-García, P.; Valbuena, G.N.; Al-Sadah, H.A.; Robinson, M.E.; Penfold, L.; Kuzeva, D.M.; Ruiz-Tellez, A.; Loaiza, S.; Holzmann, V.; et al. The coordinated action of VCP/p97 and GCN2 regulates cancer cell metabolism and proteostasis during nutrient limitation. *Oncogene* **2019**, *38*, 3216–3231, https://doi.org/10.1038/s41388-018-0651-z.
24. Fu, Q.; Jiang, Y.; Zhang, D.; Liu, X.; Guo, J.; Zhao, J. Valosin-containing protein (VCP) promotes the growth, invasion, and metastasis of colorectal cancer through activation of STAT3 signaling. *Mol. Cell. Biochem.* **2016**, *418*, 189–198, https://doi.org/10.1007/s11010-016-2746-6.
25. Zhu, Y.; Romero, M.I.; Ghosh, P.; Ye, Z.; Charnay, P.; Rushing, E.J.; Marth, J.D.; Parada, L.F. Ablation of NF1 function in neurons induces abnormal development of cerebral cortex and reactive gliosis in the brain. *Genes Dev.* **2001**, *15*, 859–876, https://doi.org/10.1101/gad.862101.
26. Jaegle, M.; Ghazvini, M.; Mandemakers, W.; Piirsoo, M.; Driegen, S.; Levavasseur, F.; Raghoenath, S.; Grosveld, F.; Meijer, D. The POU proteins Brn-2 and Oct-6 share important functions in Schwann cell development. *Genes Dev.* **2003**, *17*, 1380–1391, https://doi.org/10.1101/gad.258203.
27. Wu, J.; Williams, J.P.; Rizvi, T.A.; Kordich, J.J.; Witte, D.; Meijer, D.; Stemmer-Rachamimov, A.O.; Cancelas, J.A.; Ratner, N. Plexiform and Dermal Neurofibromas and Pigmentation Are Caused by Nf1 Loss in Desert Hedgehog-Expressing Cells. *Cancer Cell* **2008**, *13*, 105–116, https://doi.org/10.1016/j.ccr.2007.12.027.
28. Dombi E, Solomon J, Gillespie AJ, Fox E, Balis FM, Patronas N, et al. NF1 plexiform neurofibroma growth rate by volumetric MRI: relationship to age and body weight. Neurology. 2007;68(9):643-7.

© 2026 by the author(s). Distributed under a Creative Commons CC BY license.

Preprints.org (www.preprints.org) | NOT PEER-REVIEWED | Posted: 9 March 2026 doi:10.20944/preprints202603.0600.v1

29. Na, Y.; Hall, A.; Yu, Y.; Hu, L.; Choi, K.; Burgard, J.A.; Szabo, S.; Huang, G.; Ratner, N.; Wu, J. Runx1/3-driven adaptive endoplasmic reticulum stress pathways contribute to neurofibromagenesis. *Oncogene* **2023**, *42*, 1038–1047, https://doi.org/10.1038/s41388-023-02620-x.
30. Wu, J.; Keng, V.W.; Patmore, D.M.; Kendall, J.J.; Patel, A.V.; Jousma, E.; Jessen, W.J.; Choi, K.; Tschida, B.R.; Silverstein, K.A.; et al. Insertional Mutagenesis Identifies a STAT3/Arid1b/β-catenin Pathway Driving Neurofibroma Initiation. *Cell Rep.* **2016**, *14*, 1979–1990, https://doi.org/10.1016/j.celrep.2016.01.074.
31. Arumugam, N.; Gupta, V.; Jagannath, A.; Mukhopadhyay, A.; Pradhan, A.K.; Burma, P.K.; Pental, D. A passage through in vitro culture leads to efficient production of marker-free transgenic plants in Brassica juncea using the Cre–loxP system. *Transgenic Res.* **2007**, *16*, 703–712, https://doi.org/10.1007/s11248-006-9058-7.
32. Li, H.; Zhao, X.; Yan, X.; Jessen, W.J.; Kim, M.-O.; Dombi, E.; Liu, P.P.; Huang, G.; Wu, J. Runx1 contributes to neurofibromatosis type 1 neurofibroma formation. *Oncogene* **2015**, *35*, 1468–1474, https://doi.org/10.1038/onc.2015.207.
33. Wu, J.; Dombi, E.; Jousma, E.; Dunn, R.S.; Lindquist, D.; Schnell, B.M.; Kim, M.; Kim, A.; Widemann, B.C.; Cripe, T.P.; et al. Preclincial testing of Sorafenib and RAD001 in the *Nf*$^{flox/flox}$*;DhhCre* mouse model of plexiform neurofibroma using magnetic resonance imaging. *Pediatr. Blood Cancer* **2011**, *58*, 173–180, https://doi.org/10.1002/pbc.23015.
34. Hall, A.; Choi, K.; Liu, W.; Rose, J.; Zhao, C.; Yu, Y.; Na, Y.; Cai, Y.; Coover, R.A.; Lin, Y.; et al. RUNX represses *Pmp22* to drive neurofibromagenesis. *Sci. Adv.* **2019**, *5*, eaau8389, https://doi.org/10.1126/sciadv.aau8389.
35. Jousma, E.; Rizvi, T.A.; Wu, J.; Janhofer, D.; Dombi, E.; Dunn, R.S.; Kim, M.-O.; Masters, A.R.; Jones, D.R.; Cripe, T.P.; et al. Preclinical assessments of the MEK inhibitor PD-0325901 in a mouse model of neurofibromatosis type 1. *Pediatr. Blood Cancer* **2015**, *62*, 1709–1716, https://doi.org/10.1002/pbc.25546.
36. Jessen, W.J.; Miller, S.J.; Jousma, E.; Wu, J.; Rizvi, T.A.; Brundage, M.E.; Eaves, D.; Widemann, B.; Kim, M.-O.; Dombi, E.; et al. MEK inhibition exhibits efficacy in human and mouse neurofibromatosis tumors. *J. Clin. Investig.* **2012**, *123*, 340–347, https://doi.org/10.1172/jci60578.
37. Zhou, H.-J.; Wang, J.; Yao, B.; Wong, S.; Djakovic, S.; Kumar, B.; Rice, J.; Valle, E.; Soriano, F.; Menon, M.-K.; et al.Discovery of a First-in-Class, Potent, Selective, and Orally Bioavailable Inhibitor of the p97 AAA ATPase (CB-5083). J Med Chem. 2015;58(24):9480-97.
38. Williams, J.P.; Wu, J.; Johansson, G.; Rizvi, T.A.; Miller, S.C.; Geiger, H.; Malik, P.; Li, W.; Mukouyama, Y.-S.; Cancelas, J.A.; et al. Nf1 Mutation Expands an EGFR-Dependent Peripheral Nerve Progenitor that Confers Neurofibroma Tumorigenic Potential. *Cell Stem Cell* **2008**, *3*, 658–669, https://doi.org/10.1016/j.stem.2008.10.003.
39. Müller, J.; Deinhardt, K.; Rosewell, I.; Warren, G.; Shima, D. Targeted deletion of p97 (VCP/CDC48) in mouse results in early embryonic lethality. *Biochem. Biophys. Res. Commun.* **2007**, *354*, 459–465, https://doi.org/10.1016/j.bbrc.2006.12.206.
40. Arhzaouy, K.; Papadopoulos, C.; Schulze, N.; Pittman, S.K.; Meyer, H.; Weihl, C.C. VCP maintains lysosomal homeostasis and TFEB activity in differentiated skeletal muscle. *Autophagy* **2019**, *15*, 1082–1099, https://doi.org/10.1080/15548627.2019.1569933.
41. Anderson, D.J.; Le Moigne, R.; Djakovic, S.; Kumar, B.; Rice, J.; Wong, S.; Wang, J.; Yao, B.; Valle, E.; von Soly, S.K.; et al. Targeting the AAA ATPase p97 as an Approach to Treat Cancer through Disruption of Protein Homeostasis. *Cancer Cell* **2015**, *28*, 653–665, https://doi.org/10.1016/j.ccell.2015.10.002.
42. Gugliotta, G.; Sudo, M.; Cao, Q.; Lin, D.-C.; Sun, H.; Takao, S.; Le Moigne, R.; Rolfe, M.; Gery, S.; Müschen, M.; et al. Valosin-Containing Protein/p97 as a Novel Therapeutic Target in Acute Lymphoblastic Leukemia. *Neoplasia* **2017**, *19*, 750–761, https://doi.org/10.1016/j.neo.2017.08.001.
43. Costantini, S.; Capone, F.; Polo, A.; Bagnara, P.; Budillon, A. Valosin-Containing Protein (VCP)/p97: A Prognostic Biomarker and Therapeutic Target in Cancer. *Int. J. Mol. Sci.* **2021**, *22*, 10177, https://doi.org/10.3390/ijms221810177.
44. Espinoza, M.J.C.; Tucker, S.K.; Sureshkumar, S.; Gamble, M.E.; Hakim, N.L.; Orrantia, S.; Espitia, C.M.; Cruickshank-Taylor, A.B.; Wang, W.; Kelly, K.R.; et al. Harnessing p97/VCP: A Transformative AAA+

© 2026 by the author(s). Distributed under a Creative Commons CC BY license.

Preprints.org (www.preprints.org) | NOT PEER-REVIEWED | Posted: 9 March 2026 doi:10.20944/preprints202603.0600.v1

ATPase Target for Next-Generation Cancer Therapeutics. *Cancers* **2025**, *17*, 2945, https://doi.org/10.3390/cancers17182945.

45. Wang, Z.; Qiao, X.; Chen, Y.; Peng, N.; Niu, C.; Wang, Y.; Li, C.; Hu, Z.; Zhang, C.; Cheng, C. SVIP reduces IGFBP-2 expression and inhibits glioblastoma progression via stabilizing PTEN. *Cell Death Discov.* **2024**, *10*, 1–12, https://doi.org/10.1038/s41420-024-02130-z.
46. Tang, W.K.; Odzorig, T.; Jin, W.; Xia, D. Structural Basis of p97 Inhibition by the Site-Selective Anticancer Compound CB-5083. *Mol. Pharmacol.* **2019**, *95*, 286–293, https://doi.org/10.1124/mol.118.114256.
47. Zhao, Z.; Wu, M.; Zhang, X.; Jin, Q.; Wang, Y.; Zou, C.; Huang, G.; Yin, J.; Xie, X.; Shen, J. CB-5083, an inhibitor of P97, suppresses osteosarcoma growth and stem cell properties by altering protein homeostasis. **2020**, *12*, 2956–2967.
48. Zhang, T.-M.; Liao, L.; Yang, S.-Y.; Huang, M.-Y.; Zhang, Y.-L.; Deng, L.; Hu, S.-Y.; Yang, F.; Zhang, F.-L.; Shao, Z.-M.; et al. TOLLIP-mediated autophagic degradation pathway links the VCP-TMEM63A-DERL1 signaling axis to triple-negative breast cancer progression. *Autophagy* **2022**, *19*, 805–821, https://doi.org/10.1080/15548627.2022.2103992.
49. Kilgas, S.; Singh, A.N.; Paillas, S.; Then, C.-K.; Torrecilla, I.; Nicholson, J.; Browning, L.; Vendrell, I.; Konietzny, R.; Kessler, B.M.; et al. p97/VCP inhibition causes excessive MRE11-dependent DNA end resection promoting cell killing after ionizing radiation. *Cell Rep.* **2021**, *35*, 109153, https://doi.org/10.1016/j.celrep.2021.109153.
50. Le Moigne, R., Aftab, B. T., Djakovic, S., Dhimolea, E., Valle, E., Murnane, M., King, E. M., Soriano, F., Menon, M. K., Wu, Z. Y. The p97 Inhibitor CB-5083 Is a Unique Disrupter of Protein Homeostasis in Models of Multiple Myeloma. Mol Cancer Ther. 2017;16(11):2375-86.
51. Zhu, H.; Ge, F.; Dai, J.; Yang, S.; Yuan, T.; Zheng, C.; Dong, X.; Hu, R.; Zhou, T.; He, Q.; et al. Targeting VCP enhances colorectal cancer therapy through STING stabilization. *J. Immunother. Cancer* **2025**, *13*, e012652, https://doi.org/10.1136/jitc-2025-012652.
52. Leinonen, H.; Cheng, C.; Pitkänen, M.; Sander, C.L.; Zhang, J.; Saeid, S.; Turunen, T.; Shmara, A.; Weiss, L.; Ta, L.; et al. A p97/Valosin-Containing Protein Inhibitor Drug CB-5083 Has a Potent but Reversible Off-Target Effect on Phosphodiesterase-6. *J. Pharmacol. Exp. Ther.* **2021**, *378*, 31–41, https://doi.org/10.1124/jpet.120.000486.
53. Roux, B.; Vaganay, C.; Vargas, J.D.; Alexe, G.; Benaksas, C.; Pardieu, B.; Fenouille, N.; Ellegast, J.M.; Malolepsza, E.; Ling, F.; et al. Targeting acute myeloid leukemia dependency on VCP-mediated DNA repair through a selective second-generation small-molecule inhibitor. *Sci. Transl. Med.* **2021**, *13*, https://doi.org/10.1126/scitranslmed.abg1168.

Disclaimer/Publisher's Note: The statements, opinions and data contained in all publications are solely those of the individual author(s) and contributor(s) and not of MDPI and/or the editor(s). MDPI and/or the editor(s) disclaim responsibility for any injury to people or property resulting from any ideas, methods, instructions or products referred to in the content.

© 2026 by the author(s). Distributed under a Creative Commons CC BY license.